Radiation Physics and Chemistry 244 (2026) 113815

Contents lists available at ScienceDirect

Radiation Physics and Chemistry

journal homepage: www.elsevier.com/locate/radphyschem

Measurement of ^{27}Al(α, n) thick-target yields by activation and ^{27}Al(α, $n\gamma$) reaction prompt γ rays

O. Alonso-Sañudo [a,*], L.M. Fraile [a,*,1], J.A. Briz [a], A. Illana [a], J. Agramunt [b], J. Benito [a,2], M.J.G. Borge [c], M. Caballero [a], D. Cano-Ott [d], G. Cortés [e], A. Espinosa-Rodriguez [a], B. Fernández [f,g], G. García [h], V. García-Távora [h], C. Guerrero [f,g], J. Llanes [d], M. Llanos-Expósito [a], T. Martínez [d], N. Mont-Geli [e], J.R. Murias [a,3], E. Nácher [b], A. Nakbi [h], V.M. Nouvillas [a], V.V. Onecha [a,4], M. Pallás [e], A. Perea [c], A. Pérez de Rada [d], J. Sánchez-Prieto [h], V. Sánchez-Tembleque [a,5], J.L. Taín [b], A. Tarifeño-Saldivia [b], O. Tengblad [c], J.M. Udías [a], S. Viñals [h]

[a] Grupo de Física Nuclear, EMFTEL and IPARCOS, Universidad Complutense de Madrid, E-28040 Madrid, Spain
[b] Instituto de Física Corpuscular, CSIC/Universidad de Valencia, E-46071 Valencia, Spain
[c] Instituto de Estructura de la Materia, CSIC, E-28049 Madrid, Spain
[d] Centro de Investigaciones Energéticas, Medioambientales y Tecnológicas, E-28040 Madrid, Spain
[e] Institut de Tècniques Energètiques, Universitat Politècnica de Catalunya, E-08028 Barcelona, Spain
[f] Dpto. Física Atómica, Molecular y Nuclear, Universidad de Sevilla (US), E-41012 Sevilla, Spain
[g] Centro Nacional de Aceleradores, Universidad de Sevilla - Junta de Andalucía - CSIC, E-41092 Sevilla, Spain
[h] Centro de Micro-Análisis de Materiales, Universidad Autónoma de Madrid, E-28049 Madrid, Spain

ARTICLE INFO

Keywords:
Thick target yield
Gamma ray spectroscopy
(α, n) reactions
Prompt-gamma rays

ABSTRACT

This work presents a study of the ^{27}Al(α, n) reaction over an extended energy range (3.5–15 MeV) relative to previous datasets, performed at the Centro de Micro-Análisis de Materiales in Madrid. Thick-target yields were obtained from activation by the online measurement of the decay of the ^{30}P reaction product, using the recently developed Gamma-detection Array for Reaction Yield measurements. The results show good agreement with existing data and confirm the newest thick-target yields at low energies. Direct ^{27}Al($\alpha, n\gamma$)^{30}P γ-yields were measured in order to address (α, n) branches to excited states in ^{30}P. The angular dependence of the emitted prompt γ rays was investigated, revealing significant differences as a function of angle with respect to the beam direction. The results provide benchmark data for future (α, n) yield studies using online activation measurements and prompt γ-ray detection.

1. Introduction

The interest of nuclear reactions induced by alpha particles, and of (α,n) reactions specifically, spans various scientific and technological fields. Apart from their genuine interest in fundamental physics to obtain information about nuclear reaction mechanisms, (α,n) reactions have an impact in nuclear astrophysics scenarios. Reactions of light and intermediate-mass nuclei are the sources of the neutrons required for the synthesis of heavier elements through neutron capture processes, such as the slow neutron capture process (s-process) (Tain et al., 2016) and the weak rapid neutron capture process (weak r-process or α-process) (Bliss et al., 2017, 2020). Such reactions take place during the explosive carbon burning phase in massive stars or shock-driven nucleosynthesis in core-collapse supernovae. The thermonuclear reaction rates are a key ingredient in stellar models and therefore the knowledge of cross sections is needed at the relevant low energies corresponding to stellar temperatures. Regarding nuclear technologies, data on neutron production reactions are needed for the design and safety analysis of fission reactors and future fusion reactors, particularly for neutronics calculations, radiation shielding, and material activation. Specifically,

* Corresponding authors.
E-mail addresses: odetteal@ucm.es (O. Alonso-Sañudo), lmfraile@ucm.es (L.M. Fraile).
[1] Present address: CERN, CH, 1211, Geneva 23, Switzerland.
[2] Present address: INFN Laboratori Nazionali di Legnaro, I-35020, Legnaro, Italy.
[3] Present address: Diamond Light Source Ltd., Didcot, Harwell Campus, Oxfordshire, OX11 0DE, United Kingdom.
[4] Present address: Department of Radiation Oncology, MGH, Harvard Medical School, Boston, MA, 02114, USA
[5] Present address: Departamento de Bioingeniería, Universidad Carlos III de Madrid, E-28911 Leganés, Spain.

https://doi.org/10.1016/j.radphyschem.2026.113815
Received 22 January 2026; Received in revised form 8 March 2026; Accepted 15 March 2026
Available online 16 March 2026

data on (α,n) reactions are required to characterize materials and waste, including transuranic waste, for the fabrication and reprocessing of nuclear fuel, and to assess the burn-up fraction of spent nuclear fuel (Vlaskin et al., 2015).

Alpha-induced reactions have also been proposed as a diagnostic tool to characterize high-temperature, high-density plasmas in facilities such as the National Ignition Facility (NIF) and International Thermonuclear Experimental Reactor (ITER) (Bonheure et al., 2011), via the detection of neutrons or reaction products, which make it possible to map the alpha particle flux within the plasma.

Another field of research where (α,n) reactions are of high impact is rare-event experiments. For example, (α,n) reactions are the primary source of background neutrons in underground experiments for dark matter searches, neutrino oscillations, and neutrino-less double-beta decay (Mei et al., 2009). The neutron background is critical in this regard, since neutrons can mimic potential dark matter signals. Alpha particles causing (α, n) reactions originate mainly from the natural decay chains of uranium and thorium, which are present in almost all materials used for detector construction or surrounding shielding. Predicting and mitigating these backgrounds requires sophisticated simulations using Monte Carlo codes (Wilson et al., 2009), which need the energy-dependent cross sections and neutron emission spectra for (α,n) reactions on all relevant isotopes as input information. The knowledge of cross sections, and thick-target yields in particular, is essential since the alpha particles will generally fully stop within nearby materials.

Despite the existence of experimental (α,n) cross sections in the literature, the available databases show discrepancies that are not compatible with the declared uncertainties. In addition, spectroscopic information is available only for a limited number of reactions. Hence, accurate data on the neutron yield from the interaction of α particles with nuclei via (α, n) reactions are of the highest interest in this context, both because of the inconsistency of the experimental available data and of the renewed interest in technological applications (Westerdale et al., 2022; Cano-Ott et al., 2024).

The need for detailed data in a wide range of applications triggered setting up the Measurement of Alpha Neutron Yields (MANY) collaboration, whose ultimate goal is the measurement of (α, xn) production yields, reaction cross sections, and neutron energy spectra. MANY employs complementary experimental techniques for the investigation of α-induced reactions, such as neutron counting, neutron spectroscopy, activation, and gamma spectroscopy.

In this work, we focus on the ^{27}Al(α,n)^{30}P reaction by investigating thick-target yields in a wide range of energies, spanning from 15 MeV down to 3.5 MeV, close to the reaction threshold. We employ the activation method, via the measurement of positron annihilation γ rays emitted by the reaction product ^{30}P, which is performed online thanks to the capabilities of a new γ-ray detection setup. We also investigate the emission of prompt γ-ray radiation $^{27}\mathrm{Al}(\alpha, n\gamma)$ and its angular dependence with respect to the α beam direction in the laboratory frame. The aims of the investigation are: (i) to benchmark the refurbished NUC45 beam line at the Centro de Micro-Análisis de Materiales (CMAM) in Madrid, Spain Redondo-Cubero et al. (2021), and the developed experimental setup; (ii) to provide a systematic measurement of thick-target yields over a broad energy range, exploiting the available α-particle energies up to 15 MeV from the 5-MV Tandetron accelerator at CMAM; (iii) to provide new information on the $^{27}\mathrm{Al}(\alpha, n\gamma)$ reaction through the detection of prompt γ rays; and (iv) to investigate the γ-ray emission angular dependence with respect to the beam direction, which had not previously been reported in literature.

2. ^{27}Al(α,n) reaction

The $^{27}\mathrm{Al}(\alpha, n)$ reaction has been discussed in the context of neutron generation from transuranic waste, where (α, n) reactions in the waste matrix contribute to the total neutron output, which mainly arises from the spontaneous fission of ^{240}Pu and other elements (Gehrke et al., 2003). The neutron production from the $^{27}\mathrm{Al}(\alpha, n)$ reaction is specifically relevant for Al_2O_3 matrices (Gehrke et al., 2003).

In the framework of fusion plasma diagnostics, ^{27}Al has been identified as a potential target that could be used to detect alpha particles resulting from deuterium-tritium fusion in the NIF target (Cerjan et al., 2018) leading to ^{30}P from the (α, n) reaction. It also plays a role in astrophysical nucleosynthesis during core-collapse supernovae (Howard et al., 1974; Subedi et al., 2020; Brandenburg et al., 2023). The $^{27}\mathrm{Al}(\alpha, n)$ is also of interest to understand the sources of background for direct dark matter detection, where neutrons from (α,n) reactions after thorium and uranium decays are the most important component (Mei et al., 2009). The reaction $^{27}\mathrm{Al}(\alpha, n)$ has also been discussed in the context of the production of the short-lived ^{30}P isotope for medical applications (Sahakundu et al., 1979).

For practically all of the previously mentioned purposes, thick-target yields are the most relevant observable, because the emitted α-particles are fully stopped in the surrounding material. In this work we undertake the measurement of $^{27}\mathrm{Al}(\alpha, n)$ reaction by activation. Our study serves as a benchmark for other measurements of the same reaction using direct neutron counting (Mont-Geli et al., 2026), and for the commissioning of a new experimental beam line and several detector systems at the CMAM accelerator laboratory.

Prior knowledge of the $^{27}\mathrm{Al}(\alpha, n)$ reaction exists, with substantial variation in data quality and energy coverage. The available cross-section data is shown in Fig. 1. Williamson et al. (1960) present total cross-section data up to 4 MeV for the $^{27}\mathrm{Al}(\alpha, n)^{30}$P reaction obtained from reactions on an evaporated aluminium target on a thick carbon backing. The $^{13}\mathrm{C}(\alpha, n)$ background is mentioned to significantly hamper the neutron yield below the first reported resonance at 3.45 MeV down to the experimentally obtained threshold of 3056 keV. Later, Stelson and McGowan (1964) provided thick-target (α,n) yields from 5.2 to 11.0 MeV employing a neutron counting method and extending the available range towards high energies, but far from the threshold energies. In turn, Howard et al. (1974) presented data in the centre-of-mass frame in a similar range, which are characterized by larger uncertainties, and have been disregarded in nuclear astrophysics evaluations (Mohr, 2015). Flynn et al. (1978) used direct neutron counting in the energy range of approximately 3.5 to 6 MeV. Measurements with a 27 μg/cm^2 thin target revealed distinct resonant structures in the excitation function. In contrast, measurements using a 442 μg/cm^2 thick target averaged over these resonances, resulting in a smooth excitation function, which is consistent with previous results, although marginally lower. Good agreement with statistical model predictions is achieved (Flynn et al., 1978). Measurements using the activation method and the stacked-foil technique (Sahakundu et al., 1979) deviate as expected from other data sets at low energies, although they are quite consistent at higher energies. A recent measurement (Roy et al., 2025) reports cross section measurements on thin Al targets in the range 2.5 to 5.2 MeV using direct neutron counting, which provide high granularity data in the measurement range. As illustrated in Fig. 1, no cross-section data exists at high energies and the existing cross-section data show certain inconsistencies.

Thick-target yields are provided in other experiments. West and Sherwood (West and Sherwood, 1982) present data in the 3.6- to 10-MeV range using a neutron counter, while Roughton et al. (1983) employ γ counting after activation and tabulate values in a wide alpha energy range from 3.2 to 36.0 MeV. While the two measurements agree above 5 MeV, at low energies data is very sparse and the accord is not as good. To extend the available data towards lower energies, Holmqvist and Ramström (Holmqvist and Ramström, 1986) employed a method involving the irradiation of a thick ^{27}Al target in small energy steps in a beam energy range from 3.04 to 3.66 MeV. The resulting neutron yields were employed to extract the cross section. In spite of the uncertainties related to stopping powers and normalization factors (Vlaskin et al., 2015), their results exhibit a rather good agreement with the other

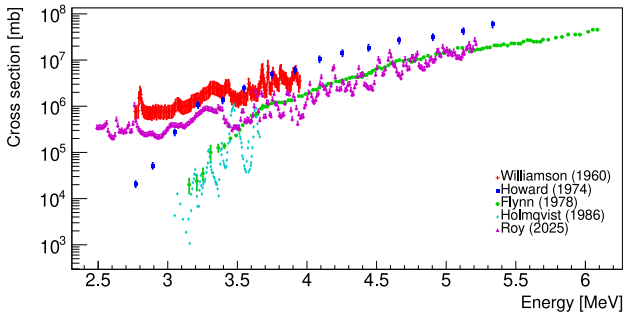

Fig. 1. Cross section data for the ^{27}Al(α, n) reaction available in literature from Howard et al. (1974), Williamson et al. (1960), Flynn et al. (1978), Holmqvist and Ramström (1986), Roy et al. (2025).

datasets across the measured range, although the region close to the energy threshold presents inconsistencies.

Brandenburg et al. (2023) focused on providing absolute thick-target yields rather than cross sections by direct neutron counting, to solve discrepancies among existing yield dataset in the 4- to 5-MeV region. Lower yields than previous measurements were obtained below 3.5 MeV. Within the MANY collaboration, a recent work at CMAM with the MiniBelen neutron counter (Mont-Geli et al., 2023b,a) with improved granularity aims to clarify existing discrepancies in literature and address the neutron background that could mask neutrons arising from the reaction. Recently, results from direct neutron counting for this reaction have been obtained by the MANY collaboration in the 3.6- to 8.5-MeV region (Mont-Geli et al., 2026).

Regarding prompt-γ-ray yields from alpha-induced reactions on light elements and from the ^{27}Al(α, n) in particular, the information is rather limited. Heaton et al. (1995, 1997) provided γ-ray yields employing two hyperpure germanium detectors positioned at forward and backward angles relative to the beam. Absolute yields for more than a dozen different γ-ray transitions in ^{30}P are given in this work for six incident α energies in the 5.6- to 10.0-MeV range. Information on other reaction channels related with this reaction (see more details on section Section 4) have also been studied by Heaton et al.

As outlined in Section 1, this work extends the energy range of thick-target yields for the ^{27}Al$(\alpha$,n$)^{30}$P reaction and provides angular distributions of the emitted prompt γ radiation.

3. Experimental details

Two experimental campaigns were performed using very similar setups and configurations. Alpha particle irradiations were done using the 5-MV terminal voltage tandem accelerator at the CMAM facility (Redondo-Cubero et al., 2021). This accelerator is a tandem type accelerator that uses the Cockroft-Walton power supply system. It is capable of delivering alpha particles up to 15 MeV with intensities up to several hundreds of nA. Two ion sources types are available at CMAM, for this experiment the duoplasmatron source was used.

The (NUC45°) beam line is connected to the 45° exit of the switching dipole magnet of the accelerator and is one of the two nuclear physics beam lines available. It has been recently upgraded and commissioned by the MANY collaboration, with the aim of investigating particle-induced reaction of astrophysical and technological interest, and for the measurement of (α, n) reaction yields, cross-section, and spectroscopic information. To that aim a new beam pipe has been designed to accommodate a versatile suite of detectors and equipped with a custom-made target holder with online current measurement capabilities (Fraile et al., 2026). To focus the beam in the target, a monitoring transparent end cap at the end of the tube was used. The aluminium targets were installed using a 3D printed support,

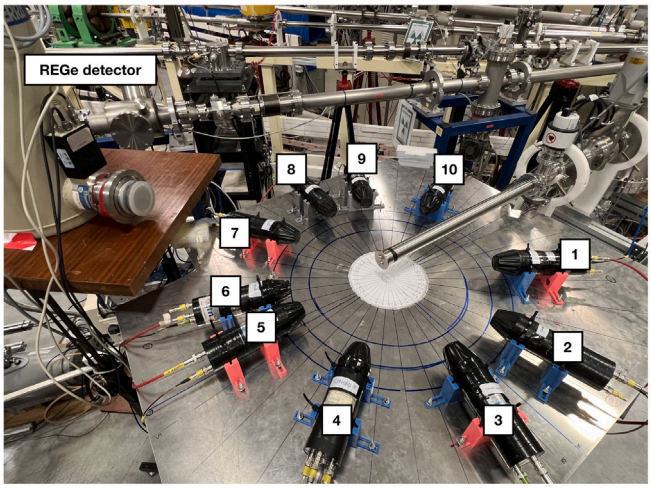

Fig. 2. Photograph of the setup used in these measurements. The distribution of the GARY $LaBr_3$(Ce) detectors with respect to the beam line and numbering is shown. The ReGE detector was placed at 45 degrees with respect to the beam direction. In the first experiment the ReGE detector was at 90 degrees instead.

encompassing the current reading and a secondary electron suppression system that was fitted to the beam pipe end cap. A tantalum collimator was used. Standard sources were placed at the implantation position for energy and efficiency calibration. Further details are provided in Fraile et al. (2026).

The target used in the experiments was a 200 μm thick aluminium foil with a purity of 99.9995% manufactured by Thermo Fisher Scientific (Thermo Fisher Scientific, 2006) placed over a tantalum backing. Since the range for 15-MeV ^{4}He particles in ^{27}Al is ∼88 μm (Ziegler et al., 2010) for normal incidence the thick-target regime is granted for any beam energy used. Under these conditions target degradation effects do not impact the measurements. In any case the beam current was maintained below 50 nA during irradiation

The Gamma-detection Array for Reaction Yield measurements (GARY), see Fig. 2, was used for both the online prompt γ and activation measurements. It consists of ten $LaBr_3$(Ce) scintillator crystals coupled to Hamamatsu R9779 photomultipliers. The crystals used have a truncated cone shape with a nominal height of 38.1 mm, and 25.4 mm and 38.1 mm diameters, respectively. They were specifically designed for fast-timing experiments (Vedia et al., 2017) and, in addition to their excellent time resolution, they are able to sustain high count rates while maintaining a reasonable energy resolution. Measurements were performed using the anode of the photomultipliers and the $LaBr_3$(Ce) detectors were operated at bias voltages between −1100 and −1200 V.

The detectors were fixed with 3D-printed supports to a metal plate and placed surrounding the target position at the end of the beam pipe. The scintillation detectors were positioned at different angles with respect to the beam direction, assuring a large angular coverage, important for the analysis of the angular dependence of the emitted prompt γ rays. Additionally, the coverage was chosen to maximize the number of different relative angles subtended by any pair of detectors. The angular arrangement as well as the distances measured from the target position to the entrance window of the crystals are shown in Table 1.

A Canberra GR3620 REGe detector with a 500-μm Be window was placed below the $LaBr_3$(Ce) array, at a 90 degree angle, at a distance of 600 ± 2 mm from the target during the first experiment. The same REGe detector was placed at the same distance but at a 45 degree angle with respect to the beam line in the second campaign, as shown in Fig. 2. This detector, having a higher resolution than the $LaBr_3$(Ce) array, makes it possible to resolve close-lying γ peaks and to identify their

Table 1
Angular distribution and distances of the GARY $LaBr_3(Ce)$ detectors with respect to the beam axis and target position.

Detector number	Angle with respect to the beam (±1)[°]	Distance to target (±2) [mm]
1	145	254
2	105	260
3	75	256
4	35	255
5	0	254
6	−15	248
7	−55	250
8	−90	255
9	−115	246
10	−155	250

reaction channels, at the expense of much lower efficiency. Calibrations in energy and efficiency were made using an absolutely calibrated ^{152}Eu (5% activity uncertainty) standard γ-ray source, positioned at the implantation point. Uncertainties regarding the source activity, the beam position and the efficiency calibration have been propagated to the experimental results. The detection efficiencies were obtained by fitting calibrated reference source data up to 1408 keV. For γ-ray energies within this range, the corresponding uncertainties were obtained through a fit to a logarithmic function with propagation of the fit parameter uncertainties. For higher energies, the fit was extrapolated and validated using Monte Carlo simulations, where detector positions were varied by ±2 mm. To account for systematic effects, the uncertainty in the extrapolated efficiency has been taken as 15%. The efficiency at 511 keV, relevant for the activation method, is not subject to extrapolation. Additionally, it has been cross-checked offline with a ^{22}Na source.

In the first campaign, signals were collected using 8-channel CAEN DT5730 digitizers (CAEN, 2025) with a sample rate of 500 MS/s and a 14-bit resolution. Each channel has a memory depth of 1024 samples, enabling full waveform capture for detailed pulse shape analysis for the fast $LaBr_3(Ce)$ scintillators. The data acquisition system used during the second experiment was a STRUCK 250 MHz 14-bit sampling digitizer (Struck Innovative Systeme, 2012). Data acquisition was controlled by GasificTL, which made it possible to save raw data and allows for on-line data monitoring (Agramunt et al., 2013).

4. Identification of reaction channels

Upon irradiation of the aluminium target with α particles different reaction channels may open up. Table 2 summarizes the threshold energy and reaction products of the different channels that may appear. Reaction on potential contaminants, such as the aforementioned tantalum, but also oxygen and iron, are included for the sake of completeness. The analysis reveals no contaminant γ lines in the spectra overlapping with those of interest. For the relevant ^{27}Al(α, n) reaction the threshold energy is ~3015 keV (Wang et al., 2021). The Coulomb barrier estimate using the standard expression for the potential energy of the electrostatic interaction with nuclei of radii $R = 1.2A^{1/3}$ fm at contact is of the order of 6.8 MeV.

Depending on the incident energy of the alpha beam, different reaction channels appear. The combined analysis of the spectra obtained with the GARY array and the REGe detector allowed the unambiguous identification of several gamma rays associated with different reaction channels. The high resolution of the REGe detector was the crucial factor in disentangling transitions close in energy, which result in partial overlap in the GARY spectra due to the limited energy resolution of $LaBr_3(Ce)$ detectors. This combination of detectors allows not only to identify reaction channels at different energies, but also to assign the detected γ rays to the particular excited levels of each product nuclei. In Fig. 3 spectra for two different beam energies, 8.5 and 15 MeV, are

Table 2
Reaction channels and their threshold energy (Wang et al., 2021) for alpha irradiation on a natural aluminium target. Reactions of potential contaminants are included for completeness. See text for more details.

Reaction channel	Product $T_{1/2}$	Threshold energy [keV]
^{27}Al$(\alpha,\gamma)^{31}$P	stable	0
^{27}Al$(\alpha,p)^{30}$Si	stable	0
^{27}Al$(\alpha,\alpha')^{27}$Al	stable	0
^{27}Al$(\alpha,n)^{30}$P	**2.498(4) min**	**3014.81(9)**
^{27}Al$(\alpha,d)^{29}$Si	stable	6859.94(5)
^{27}Al$(\alpha,t)^{28}$Si	stable	9388.67(5)
^{27}Al$(\alpha,p\alpha)^{26}$Mg	stable	9436.96(6)
^{27}Al$(\alpha,2\alpha)^{23}$Na	stable	11514.18(5)
^{27}Al$(\alpha,2p)^{29}$Al	6.56(1) min	12712.40(4)
^{12}C$(\alpha,n)^{15}$O	122.24(5) s	2754.0(1)
^{13}C$(\alpha,n)^{16}$O	stable	2215.0(1)
^{16}O$(\alpha,n)^{19}$Ne	17.22(5) s	3529.0(1)
^{56}Fe$(\alpha,n)^{59}$Ni	$7.6{\cdot}10^4$(1) y	5422.90(5)
^{181}Ta$(\alpha,n)^{184}$Re	38.0(1) d	10009.00(5)

presented. The comparison of both spectra makes clear the opening of different reaction channels as a function of energy through the emergence of new γ rays, which have been classified by their channel of origin.

Prompt γ rays from four different reaction channels are observed (see Fig. 3). The level scheme of ^{30}P is shown in Fig. 4. Seven γ rays from the ^{27}Al$(\alpha, n)^{30}$P channel that had already been identified by Heaton et al. (1997) are observed at 2131, 2260, 2342, 2474, 2538, 2724, and 2840 keV. Many other γ rays from this reaction are labelled in Fig. 3. For the ^{27}Al$(\alpha, p)^{30}$Si channel, five γ rays have been found in common with Heaton et al. (1997) at 2235, 2996, 2597, 3252, and 3379 keV, but the combination of the REGe detector and GARY allows us to identify many more. The other two relevant reactions are ^{27}Al$(\alpha, \alpha')^{27}$Al and ^{27}Al$(\alpha, d)^{29}$Si.

5. Experimental procedure

Measurements performed in both campaigns consisted of a beam-on phase, in which the sample is irradiated and activated, and a beam-off phase in which the decay is measured for a few ^{30}P lifetimes, see Table 3 and Fig. 5.

The alpha particle flux was monitored online by reading out the current on the metallic aluminium target to an ORTEC 439 Digital Current Integrator, whose output was fed to the DAQ and digitized. It was verified that it remained stable during each individual measurement. The total charge was integrated and the statistical error propagated to the yield calculations.

The activation product from the ^{27}Al(α, n) reaction, ^{30}P, decays mostly by β^+ decay with a very small electron capture branch (0.144%), with a half-life of $T_{1/2}$ = 149.88(24) s. The decay mostly populates the ^{30}Si ground state with a 99.804% branch. The ^{30}Si excited states are almost not fed, the most intense β-delayed γ-ray emission coming from 2^+ level at 2235 keV with relative intensity of 0.059(3)%. Therefore the main γ-ray emission comes from positron annihilation at 511 keV, with a relative intensity (branching ratio) of 199.712(8)%. The 511-keV γ peak is therefore the one used to obtain the thick target yields by activation. The β^+-decay lifetime provides unambiguous identification of the decaying nucleus. Additionally, no other β^+ emitter has been identified in the spectra measured after irradiation.

Gamma rays emitted during beam irradiation are monitored online. In the absence of dead time effects, the irradiation phase can be used for prompt γ-ray analysis, but also for activation using the 511-keV γ ray, as discussed below.

The set of measurements performed during both experimental campaigns is summarized in Table 3. The nominal energy uncertainty for

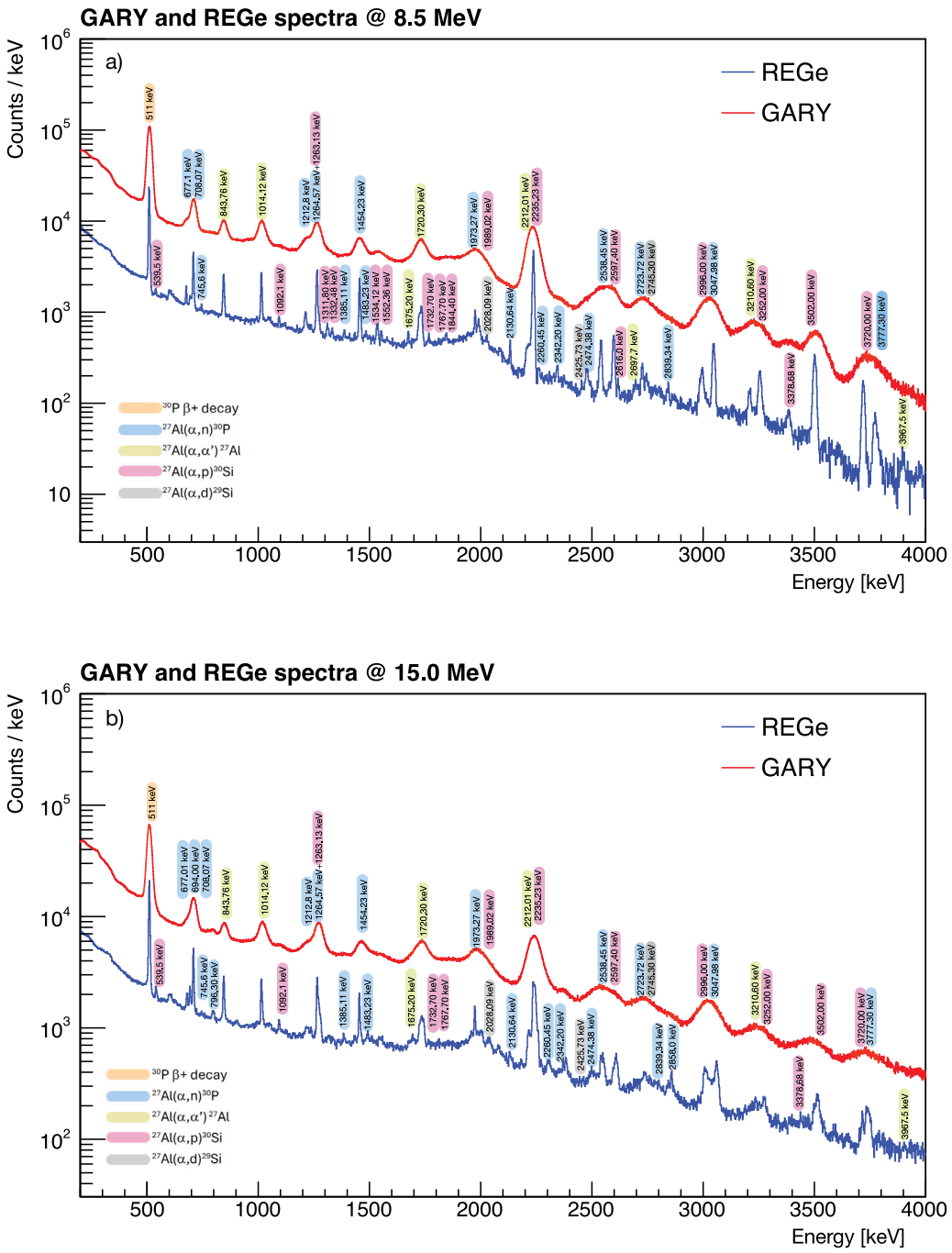

Fig. 3. Energy spectra obtained during irradiation at beam energies of (a) 8.5 and (b) 15 MeV using the $LaBr_3$(Ce) array (red) and the REGe detector (blue). The identified prompt γ rays from the different reaction channels are shown: shaded in light blue the channel of main interest ^{27}Al(α, (n) ^{30}P, in orange the ^{30}P β+ decay, in green, pink, and grey the ^{27}Al(α, α')^{27}Al, ^{27}Al(α,p)^{30}Si, and $Al(\alpha,p)^{31}$Si reaction channels, respectively. γ-ray energies have been taken from National Nuclear Data Center (2025).

proton beams at the facility is estimated to be less than 3 keV (Bachiller-Perea et al., 2013). A comparable energy uncertainty for doubly-charged alpha particles under similar operational conditions is assumed.

Thick-target yield by activation can be calculated as follows:

$$Y = \frac{A_{irr}}{\phi(1 - e^{-\lambda t_{irr}})} \tag{1}$$

where A_{irr} is the activity after irradiation, t_{irr} is the time while the sample is being irradiated, ϕ represents the alpha particle flux and λ is the decay constant. The sample activity after irradiation can be then calculated by using the expression:

$$A_{irr} = \lambda \frac{N_\gamma}{\epsilon_\gamma br_\gamma} \frac{e^{\lambda t_{wait}}}{(1 - e^{-\lambda t_{meas}})} \tag{2}$$

t_{wait} being the time span from the end of irradiation to the start of the measurement.

Therefore the thick-target yield can be written by:

$$TTY = \frac{N_\gamma}{\epsilon_\gamma br_\gamma} \frac{\lambda}{\phi} \frac{e^{\lambda t_{wait}}}{(1 - e^{-\lambda t_{meas}})(1 - e^{-\lambda t_{irr}})} \tag{3}$$

where N_γ stands for the number of counts measured for a γ peak, in our case 511 keV, ϵ_γ represents the full-energy peak efficiency of the

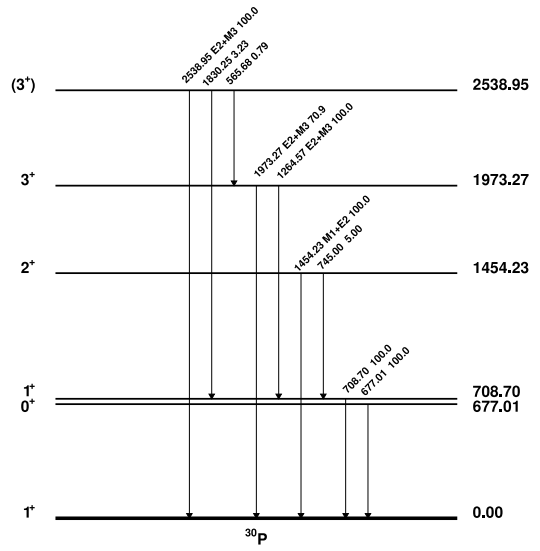

Fig. 4. Gamma transitions in ^{30}P leading to prompt γ ray emission from the ^{27}Al$(\alpha,n)^{30}$P reaction. Data from National Nuclear Data Center (2025).

Table 3
Energy, irradiation time and intensity values extracted from the measurements of both experiments performed at CMAM. The statistical error in time measurement is one second for both time measurements. Errors in the integrated charge follow standard error propagation.

Beam Energy (MeV)	Irradiation time (±1) [s]	Decay time (±1) [s]	Integrated charge [μC]
3.60	1199	1497	117(1)
3.80	1173	127	99(1)
4.00	894	1227	95(1)
4.50	800	1212	27.1(5)
5.00	983	1500	27.8(5)
5.20	850	150	21.7(5)
5.30	520	100	12.5(4)
5.40	461	520	10.4(3)
5.60	1653	1950	63.3(8)
6.00	493	20	20.7(5)
6.50	680	–	23.5(5)
6.50	917	1181	81(1)
6.75	2275	2150	74(1)
7.00	840	120	25.0(5)
7.50	850	1470	23.3(5)
8.00	570	–	13.7(4)
8.50	740	120	14.0(4)
10.00	834	1739	66.7(8)
12.00	592	1768	19.8(4)
14.00	716	1543	7.8(3)
15.00	647	202	6.5(3)

detector at this energy, br_γ represents the gamma branching ratio of the analysed peak and finally t_{meas} is the measurement time, see Fig. 5.

Thanks to the online measurement capability, we can obtain data not only during the decay period of the sample, but also while monitoring the irradiation. In fact, we can distinguish three ways of calculating the activity of the sample. Firstly, the activity can be directly calculated using the total number of counts accumulated during the measurement time (t_{meas}), comprising both the irradiation (t_{irr}) and decay (t_{decay}) phases, see Fig. 5. In the limit $t_{decay} \gg T_{1/2}$ no correction is required. Else a decay correction will be necessary. Secondly, the decay period (t_{decay}) can only be used, by applying the necessary correction due to the decay of the activity during the irradiation phase. Finally, it is also possible to use the activity growth during the irradiation phase (t_{irr}), Fig. 5, taking into account the decay during irradiation and correcting for beam current instabilities when required. These three different ways of measuring the produced ^{30}P activity resulted in compatible yield

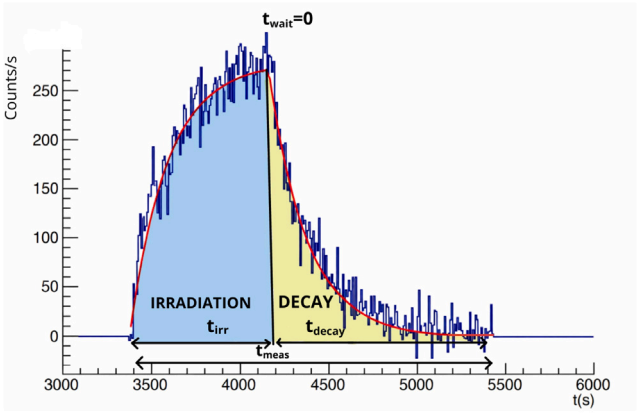

Fig. 5. Irradiation (t_{irr}) and decay (t_{decay}) phases observed online for the 511-keV γ-ray peak. t_{meas} represents the total measurement time and t_{wait} the time interval between the irradiation measurement and the decay measurement, which is zero in the example.

results, but we have employed the first method, when possible, since it requires less corrections. Potential dead time effects were considered in the data analysis. At the highest beam energy the peak counting rate was 20 kHz. The comparison of the measured activity during irradiation and decay under these conditions revealed that dead time was still negligible.

To obtain prompt γ-ray yields for the ^{27}Al$(\alpha,n\gamma)$ reaction the irradiation period is obviously employed by measuring the online count rate of γ lines from the prompt de-excitation spectra of ^{30}P (see Fig. 4), and correcting by the full-energy peak efficiency.

6. Thick target (α,n) yields

The thick target yields presented in this work have been measured using the sum of the irradiation and decay time, t_{meas} as discussed. For a few beam energies, when no decay measurements were performed, only the irradiation phase, t_{irr}, was used, see Table 3. In every case, uncertainties have been calculated and propagated. The integrated charge with its uncertainty is given in Table 3, and it is typically below 3%. The main source of error is the efficiency at 511 keV, mostly stemming from the absolute efficiency of the calibration source, and, for the lowest beam energies, the statistical uncertainty in the number of detected counts.

Thick target yields using GARY and the REGe detector in a range of energies from 3.5 to 15 MeV are shown in Table 4 and Fig. 6.

Fig. 7 shows thick target yields for 4 different existing datasets including direct neutron counting (West and Sherwood, 1982; Brandenburg et al., 2022; Mont-Geli et al., 2026) and activation (Roughton et al., 1983), compared to the results obtained in this work. Our new data closely matches the results presented in West and Sherwood (1982) and Brandenburg et al. (2022), which confirms that the online activation procedure is a viable method to measure yields. Up to beam energies of 10 MeV the same is true if we compare the data from this campaign with those from Roughton et al. (1983). However, at higher energies the GARY and REGe data tend to lie at the upper end of the range of yields, suggesting possible slightly higher yields in this region compared to some of the previous measurements. Collectively, these datasets show a remarkable consistency, considering the different types of experiments (West and Sherwood, 1982; Brandenburg et al., 2022), which provide as a solid benchmark. Apart from confirming prior results down to energies below 4 MeV, our measurements extend to energies close to 15 MeV, providing a consistent data set over an extended energy range. Reaction-model calculations based on statistical approaches such as the Hauser–Feshbach formalism, are widely used

Table 4
Activation yields obtained in both experimental campaigns for the different detectors used.
*Average value for two 6.5-MeV measurements. See text for details.

Beam Energy [MeV]	GARY Yield [10^{-6}]	REGe Yield [10^{-6}]
3.60	0.0056(11)	0.0055(11)
3.80	0.0126(15)	0.0103(13)
4.00	0.0157(10)	0.0167(22)
4.50	0.074(11)	0.064(9)
5.00	0.29(4)	0.336(18)
5.20	0.37(5)	0.426(23)
5.30	0.41(6)	0.48(3)
5.40	0.54(8)	0.61(3)
5.60	0.71(10)	0.91(5)
6.00	1.44(21)	1.57(8)
6.50*	2.00(3)	2.6(3)
6.75	3.2(4)	3.92(20)
7.00	3.6(5)	4.38(22)
7.50	6.1(9)	5.3(3)
8.00	7.0(10)	7.4(4)
8.50	10.9(16)	13.2(7)
10.00	33.2(21)	39(4)
12.00	65(10)	56(7)
14.00	112(20)	93(12)
15.00	166(20)	172(22)

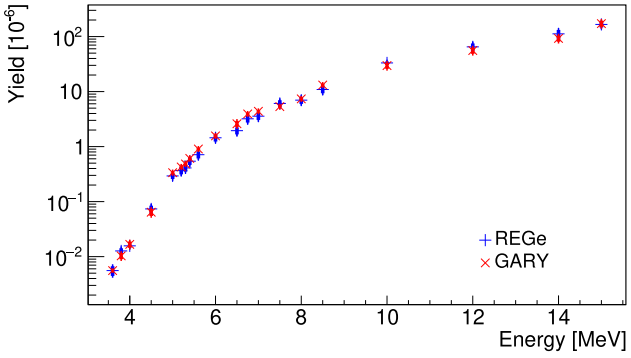

Fig. 6. Total yields obtained in both experimental campaigns in a range of energies from 3.5 to 15 MeV for both detector systems.

to predict absolute cross sections and are implemented in codes such as TALYS (Koning et al., 2019) and EMPIRE (Herman et al., 2007). Since the present work reports γ-ray yields rather than absolute cross sections, a direct comparison with yields obtained from calculated cross sections and beam energy losses is not presented here.

7. Prompt $(\alpha, n\gamma)$ γ-ray yields

Prompt γ-ray yields from the $(\alpha, n\gamma)$ reaction were extracted from the analysis of the γ-ray transitions of interest during irradiation. Yields can be obtained either using the GARY-array or the REGe detector. The results extracted from these systems are compatible with each other.

Due to the nuclear reaction by the α particles on the ^{27}Al (J^{π}=5/2^{+}) target polarization is induced. This leads to anisotropic γ-ray emission from ^{30}P reaction product with respect to the preferential direction defined by the beam. Extracted prompt γ-ray yields using the counts for a gamma peak integrated over the angles subtended by the individual detectors of GARY will be systematically biased, since the distribution of detectors is not isotropic (see Table 1), and the angle of emission with respect to the beam direction is not taken into account. Similarly, the REGe detector is positioned at a particular angle with respect to the beam direction. With this in mind the geometric configuration of the GARY array (see Fig. 2) was designed to ensure sensitivity to the angular dependence of the γ rays emitted in the reaction.

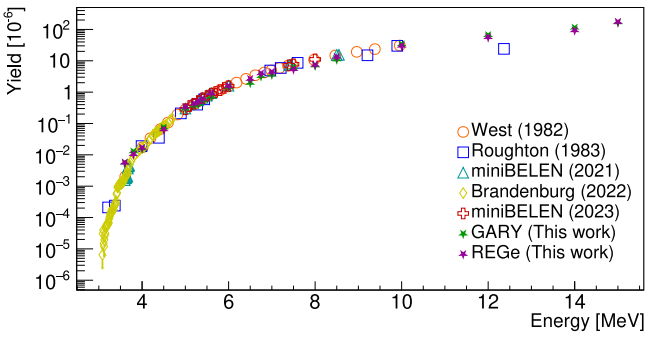

Fig. 7. Total yields obtained in both experimental campaigns and for both GARY and REGe, compared to previous works. Data from West and Sherwood (West and Sherwood, 1982), miniBELEN (Mont-Geli et al., 2026) and Brandenburg (Brandenburg et al., 2022) were obtained using a neutron counter, while the data reported by Roughton (Roughton et al., 1983) were determined via γ counting following activation. See text for details..

Table 5
Coefficients of the Legendre polynomial of angular correlations obtained for different γ rays for different beam energies.

E_γ [keV] Reaction Channel	Beam Energy [MeV]	a_0 [10^{-6}]	a_1 [10^{-6}]	a_2 [10^{-6}]
677.0 (α,nγ)	6.50	0.050(14)	0.15(8)	−0.11(8)
	6.75	0.07(3)	0.30(20)	−0.29(21)
	7.00	0.121(18)	0.17(0.13)	−0.07(14)
708.7 (α,nγ)	6.50	0.50(4)	1.5(3)	−1.3(3)
	6.75	0.72(17)	1.6(13)	−1.4(13)
	7.00	0.91(7)	1.9(5)	−1.7(5)
843.0 (α, $\alpha'\gamma$)	6.50	0.24(3)	0.29(17)	−2.4 (18)
	6.75	0.34(3)	0.3(2)	−2.75(20)
	7.00	0.43(4)	0.4(3)	−0.4(3)

The angular distribution of the emitted γ rays can be expressed as an expansion of even Legendre polynomials, $W(\theta) = 1 + b_2 P_2(\cos\theta) + b_4 P_4(\cos\theta)$ (Krane et al., 1973; Seyler and Weller, 1979; Birstein et al., 1968). The coefficients b_2 and b_4 include the preferential population of the magnetic substates of the excited nuclear level along the beam direction and the intrinsic angular distribution of the γ transition, given by its multipolarity. Using the expansion of the Legendre polynomials, the angular dependence takes the form:

$$W(\theta) = a_0 + a_1 cos^2(\theta) + a_2 cos^4(\theta) \quad (4)$$

where θ represents the angle of the detector with respect to the beam axis. The a_L coefficients encompass the spin alignment and multipolarity information of the nuclear states and transitions involved. In particular, the a_0 coefficient corresponds to the angle-integrated component and will be taken as the γ-ray yield.

A clear anisotropy in the gamma emission is observed for the γ rays at 677.0 and 708.7 keV, and it can be modelled as a function of $cos^2(\theta)$ as shown in Fig. 9. The coefficients of the polynomial expansion in $cos^2(\theta)$ are summarized in Table 5 for three different beam energies. The 843.0-keV γ ray from the (α, $\alpha'\gamma$) channel also shows an angular dependence, and is included for completeness. The anisotropy is most pronounced in the (α,nγ) peaks, particularly for the 708.7-keV γ ray. As the energy increases, the angular distribution becomes influenced by indirect γ feeding from higher-lying states that are populated in the reaction.

While the identification of γ peaks is aided by the ReGE, the poor energy resolution of the $LaBr_3$(Ce) detectors limits this approach, such that angle-dependent yield corrections can only be reliably obtained in

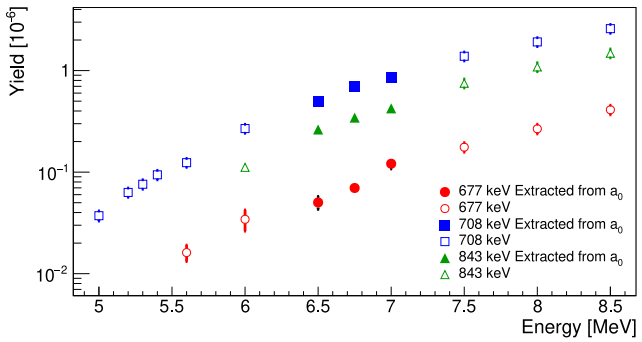

Fig. 8. γ-ray yields obtained for the γ rays of 677 and 708 keV from (α,nγ) reaction channel and the 843-keV γ ray from (α, α' γ) reaction channel corrected for angular dependence. γ-ray yields at beam energies of 6.5, 6.75, and 7 MeV were directly extracted from a_0, while the yields at other energies were normalized using a correction factor derived from a_0. Only γ-ray yields that were resolved with GARY array are shown.

Table 6
Gamma Yields measured from ($\alpha, n\gamma$) reaction channel using the REGe detector placed at 90°.

Beam Energy [MeV]	γ-ray yield [10^{-6}]				
	677 keV	708 keV	1973 keV	2131 keV	2538 keV
5.00	–	0.037(4)	–	–	–
5.20	–	0.063(6)	–	–	–
5.30	–	0.076(8)	–	–	–
5.40	–	0.094(10)	–	–	–
5.60	0.016(3)	0.124(12)	–	–	–
6.00	0.034(9)	0.27(3)	–	–	–
6.50	0.050(7)	0.50(5)	–	–	0.131(23)
6.75	0.070(7)	0.70(7)	0.24(4)	–	0.19(3)
7.00	0.121(14)	0.86(9)	0.32(5)	0.071(24)	0.32(5)
7.50	0.176(19)	1.38(14)	0.47(8)	0.11(3)	0.60(1)
8.00	0.27(3)	1.92(20)	0.84(14)	0.20(4)	0.99(15)
8.50	0.41(4)	2.6(3)	0.88(14)	0.37(7)	1.37(21)

a limited number of cases as shown in Fig. 8. But otherwise averaged prompt γ yield values can be procured from the combined GARY spectrometer. Because the distribution of the GARY $LaBr_3$ detectors is not isotropic, these angle-averaged yield values may differ from the actual yields. A normalization factor can be derived for the identified γ rays from the a_0 coefficient of the polynomial expansion listed in Table 5. Assuming that the dependence on the beam energy is negligible, the correction can be applied to γ-ray yields at energies where the limited energy resolution of the GARY array prevents a direct extraction of the angular dependence.

Additionally, the REGe detector, which does not need to be corrected by angular dependence since it was placed at 90 ° with respect to the beam line in the first campaign, can be used. Table 7 includes the yield values obtained for other γ rays, where angular distributions cannot be measured. In all cases they have been obtained from the REGe detector. For some of them a comparison can be established with previous data from Heaton et al. (1997) (see Table 6). Fig. 11 shows a comparison of the γ- ray yields resulting from both experimental campaigns and the ones obtained by Heaton et al. (1997). Our data has a much larger granularity and extends to lower beam energies. In general data are compatible with the previous values. Nonetheless, we consistently report somewhat greater yields at 2538.4 keV, and the discrepancies become more noticeable for the 2130.6-keV γ- ray yields, which may be due to how close peaks are in that region, see Fig. 3. There is also information for 2235.2-, 2597.4-, and 3252.0-keV γ-ray yields from the ($\alpha, p\gamma$) reaction, which are also consistent with literature (Heaton et al., 1997) (see Fig. 10).

Table 7
Gamma yields measured from the (α,p γ) and ($\alpha, \alpha'\gamma$) reaction channels using the REGe detector placed at 90° degrees.

Beam Energy [MeV]	γ-ray yield [10^{-6}]				
	843 keV (α, $\alpha'\gamma$)	1014 keV (α, $\alpha'\gamma$)	2235 keV (α,pγ)	2597 keV (α, pγ)	2996 keV (α, pγ)
4.00	–	–	0.071(14)	–	–
5.00	–	–	0.25(4)	–	–
5.00	–	–	0.60(9)	–	–
5.20	–	–	0.86(13)	–	–
5.30	–	–	1.01(15)	–	–
5.40	–	–	1.20(18)	–	–
5.60	–	–	1.51(23)	–	–
6.00	0.112(9)	–	1.3(3)	–	–
6.50	0.26(3)	0.0120(10)	3.4(5)	0.34(5)	0.19(3)
6.75	0.34(4)	0.0187(12)	4.4(7)	0.44(7)	0.23(4)
7.00	0.43(5)	0.0239(17)	5.4(8)	0.53(8)	0.33(5)
7.50	0.75(8)	0.044(3)	7.7(15)	0.824(13)	0.49(8)
8.00	1.09(11)	0.072(5)	10.2(15)	1.20(19)	0.791(13)
8.50	1.48(15)	0.10(7)	13.0(20)	1.52(23)	1.01(6)

Beam Energy [MeV]	γ-ray yield [10^{-6}]			
	3211 keV (α, $\alpha'\gamma$)	3252 keV (α,pγ)	3502 keV (α, pγ)	3720 keV (α,pγ)
5.60	–	0.050(9)	0.19(3)	–
6.00	–	0.099(19)	0.28(5)	–
6.50	–	0.18(3)	0.48(7)	0.06(11)
6.75	–	0.24(4)	4.56(9)	0.106(16)
7.00	0.076(21)	0.33(5)	0.67(10)	0.15(3)
7.50	0.15(3)	0.49(8)	0.92(14)	0.35(9)
8.00	1.20(4)	0.64(10)	1.32(20)	0.55(9)
8.50	0.35(6)	0.88(14)	1.7(3)	0.840(13)

Conclusions

In this work we present the measurement by activation of ^{27}Al(α,n)^{30}P thick-target yields in a wide 3.5–15 MeV energy range. The experiments were performed at the Centro de Micro-Análisis de Materiales in Madrid. The decay of the ^{30}P activation product was measured online taking advantage of the $LaBr_3$(Ce)-based Gamma-detection array for Alpha-induced Reaction Yield measurements (GARY). The obtained thick-target yield results show consistency with most existing datasets (West and Sherwood, 1982; Roughton et al., 1983) and in particular with the latest thick-target yields obtained at low energies by neutron counting (Brandenburg et al., 2022). In addition, new data have been obtained at higher beam energies than those previously reported. The extraction of cross sections from the thick-target yields reported here is not straightforward, since a much finer beam energy spacing would have been required. Within the MANY collaboration, cross sections were derived from TTY via direct neutron counting (Mont-Geli et al., 2023a, 2026), providing the reaction rates for each beam energy. This method, however, might be more sensitive to background from target contaminants than activation measurements.

Additionally, ^{27}Al($\alpha, n\gamma$)^{30}P γ yields were measured in order to access (α,n) branches to excited states in ^{30}P. The identification of emitted γ rays was achieved by combining the high count-rate capability of the GARY array with the excellent energy resolution of a REGe detector. In the ($\alpha, n\gamma$) reaction up to seven γ rays could be measured. Other reaction channels were identified as well.

The angular distribution of the emitted prompt γ rays was investigated with GARY, when possible. The γ yields show a significant dependence on the detection angle with respect to the beam direction, which was described using Legendre polynomials.

In particular, the 677- and 708-keV γ rays of the (α,nγ) channel and the 843-keV γ ray of the (α, $\alpha\gamma$) channel could be measured at several beam energies, highlighting the angular dependence of the emitted electromagnetic radiation. Very sizeable effects up to 70% can be observed in some cases. The angular dependence is diluted as

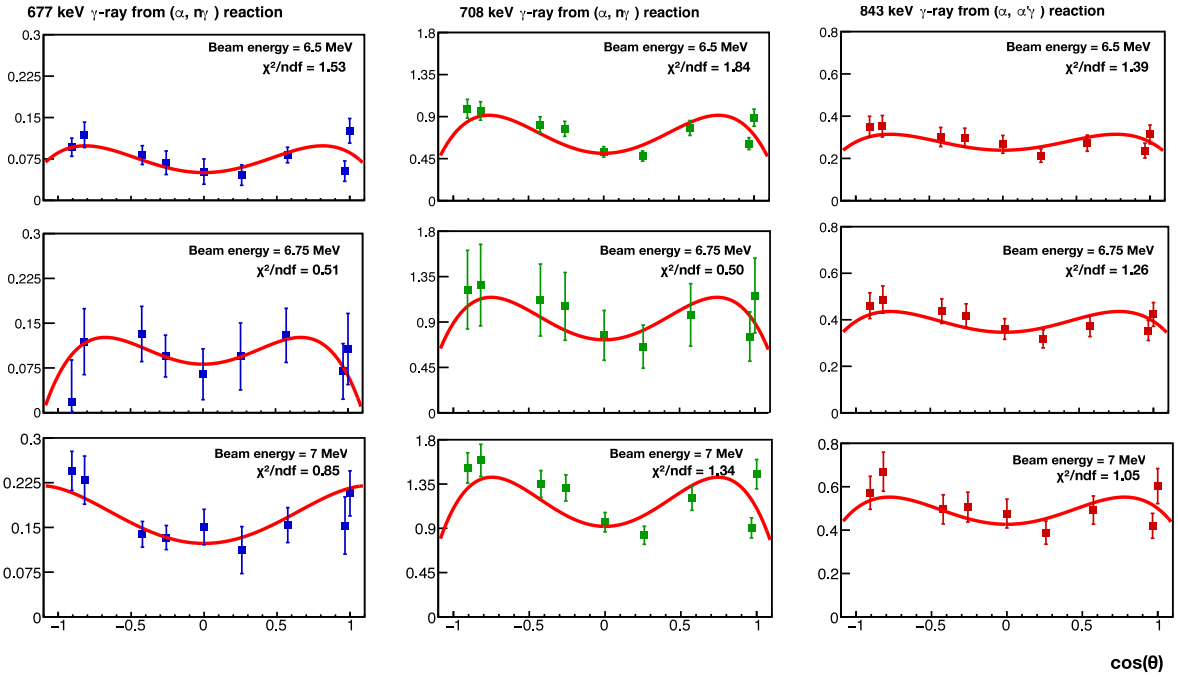

Fig. 9. Angular dependence observed at different beam energies for the 677.0- and 708.7-keV γ rays from the (α,nγ) reaction channel and the 843.0-keV γ ray from the (α, $\alpha'\gamma$) reaction channel.

the beam energy is increased, due to the contribution from indirect feeding of higher-lying states, but the anisotropy in the emission is still present. Gamma-yields have been obtained from the fit to the angular distributions for the available γ rays. For the energies where angular dependence could not be measured the corrected averaged value from GARY has been used. Values from the REGe detector have also been obtained for 5 additional prompt γ rays for an extended α beam energy range. The γ yields have been found to be generally in good agreement with those reported by Heaton et al. (1997). A more extensive data set is obtained in the present work.

In conclusion, this work provides thick-target yields measured by activation for the ^{27}Al(α,n)^{30}P reaction in an extended energy range up to 15 MeV. The results are in good agreement with neutron counting experiments (Mont-Geli et al., 2026) (Brandenburg et al., 2022), providing benchmark data for this type of measurements with GARY at the refurbished NUC45 ° beam line at CMAM. Prompt γ-ray yields from the ^{27}Al(α,n γ)^{30}P reaction were also measured in a wide energy range for a comprehensive set of γ-ray energies, using both GARY and a REGe detector. For the first time, the angular distribution of the γ-ray emission for this reaction was investigated, revealing sizeable effects depending on the angle with respect to the beam direction. This may have consequences for the design of experimental setups, particularly regarding the placement of detectors at fixed locations.

Future alpha-induced reaction studies or this kind are already underway or planned by the MANY collaboration at CMAM.

CRediT authorship contribution statement

O. Alonso-Sañudo: Writing – original draft, Methodology, Investigation, Formal analysis. **L.M. Fraile:** Writing – review & editing, Supervision, Resources, Project administration, Investigation, Conceptualization. **J.A. Briz:** Writing – review & editing, Supervision, Methodology, Investigation. **A. Illana:** Writing – review & editing, Supervision, Investigation. **J. Agramunt:** Investigation. **J. Benito:** Investigation. **M.J.G. Borge:** Supervision, Investigation. **M. Caballero:** Investigation. **D. Cano-Ott:** Investigation. **G. Cortés:** Investigation. **A. Espinosa-Rodriguez:** Methodology, Investigation. **B. Fernández:** Investigation. **G. García:** Supervision, Methodology, Investigation. **V. García-Távora:** Investigation. **C. Guerrero:** Investigation. **J. Llanes:** Investigation. **M. Llanos-Expósito:** Investigation. **T. Martínez:** Investigation. **N. Mont-Geli:** Methodology, Investigation. **J.R. Murias:** Methodology, Investigation. **E. Nácher:** Investigation. **A. Nakbi:** Methodology, Investigation. **V.M. Nouvillas:** Methodology, Investigation. **V.V. Onecha:** Investigation. **M. Pallás:** Methodology, Investigation. **A. Perea:** Investigation. **A. Pérez de Rada:** Investigation. **J. Sánchez-Prieto:** Investigation. **V. Sánchez-Tembleque:** Investigation. **J.L. Taín:** Investigation. **A. Tarifeño-Saldivia:** Methodology, Investigation. **O. Tengblad:** Investigation. **J.M. Udías:** Investigation, Funding acquisition. **S. Viñals:** Methodology, Investigation.

Declaration of competing interest

The authors declare that they have no known competing financial interests or personal relationships that could have appeared to influence the work reported in this paper.

Acknowledgements

This work was funded by the Spanish MCIN/AEI/501100011033 under grants TED2021-130592B-I00 PROTOTWIN and PID2021-12 6998OB-I00. We acknowledge the support by the HISTARS CERN-MRR project funded by the Spanish MCIN and the European Union NextGenerationEU RRF. The authors also acknowledge the support from The Centro de Microanálisis de Materiales (CMAM) – Universidad Autónoma de Madrid, for the beam time, and its technical staff for their contribution to the operation of the accelerator. This is a contribution for the Moncloa Campus of International Excellence, “Grupo de Física Nuclear-UCM”, Ref. [910059].

Data availability

Data will be made available on request.

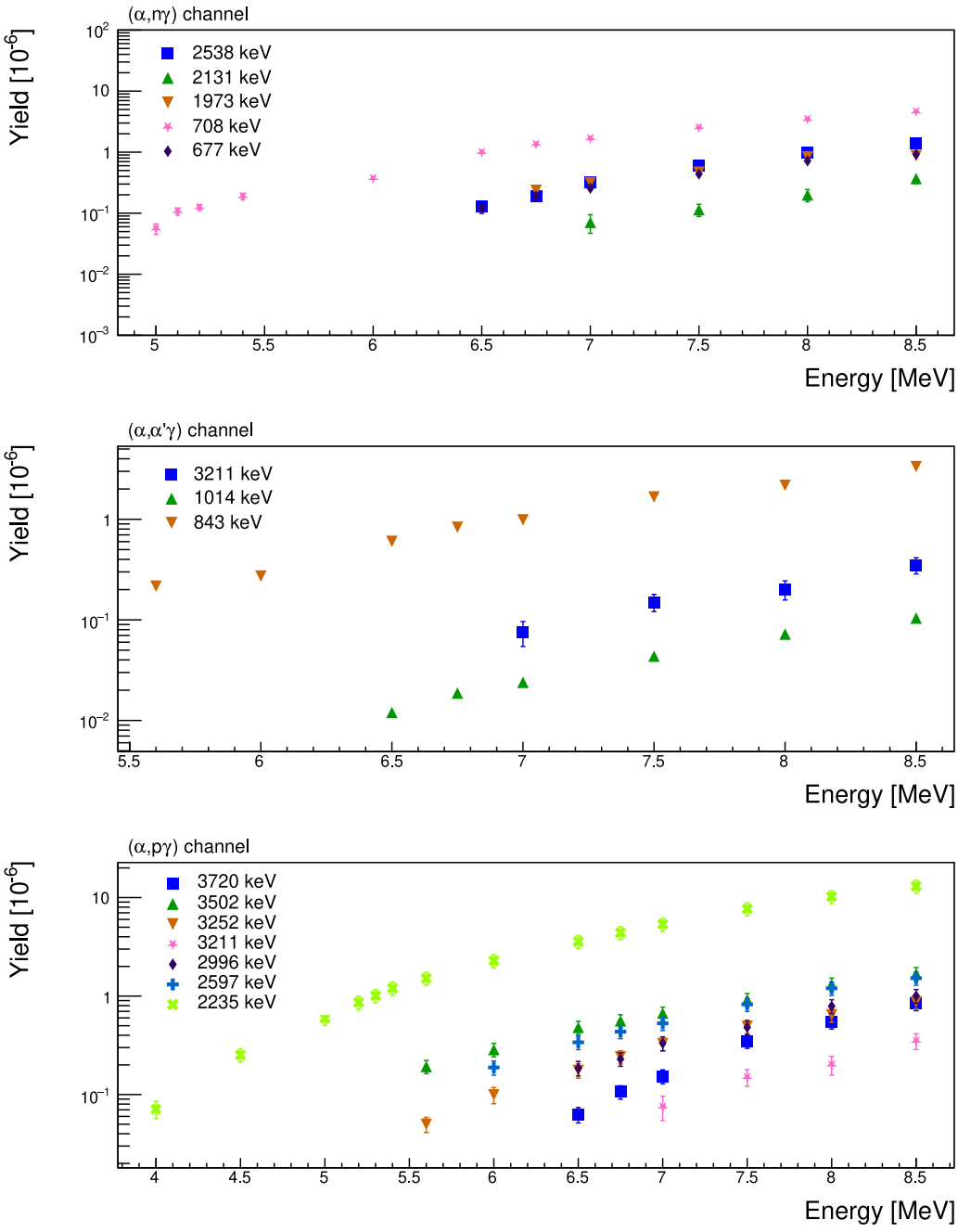

Fig. 10. γ-ray yields obtained using the REGe detector during the first experiment.

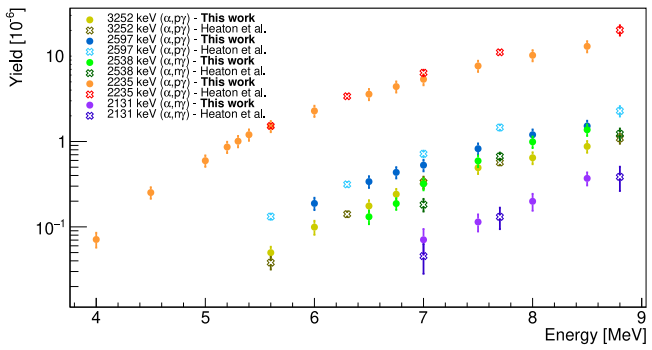

Fig. 11. Comparison between the γ-ray yields obtained by Heaton et al. (1997) and this work. In bold, γ-ray yields from the $(\alpha, n\gamma)$ channel.

References

Agramunt, J., Tain, J.L., Albiol, F., Algora, A., Estevez, E., Giubrone, G., Jordan, M.D., Molina, F., Rubio, B., Valencia, E., 2013. A triggerless digital data acquisition system for nuclear decay experiments. AIP Conf. Proc. 1541, 165–166. http://dx.doi.org/10.1063/1.4810829.

Bachiller-Perea, D., Munoz-Martin, A., Corvisiero, P., Jimenez-Rey, D., Joco, V., Maira, A., Nakbi, A., Rodriguez, A., Narros, J., Zucchiatti, A., 2013. New Energy Calibration of the CMAM 5MV Tandem Accelerator. Energy Procedia 41, 57–63. http://dx.doi.org/10.1016/j.egypro.2013.09.007, International workshop Energy 2012.

Birstein, L., Chechik, R., Drory, C., Friedman, E., Jaffe, A.A., Wolf, A., 1968. The angular distributions of gamma rays following (α,n) and (p,n) reactions. Nucl. Phys. A 113 (1), 193–205. http://dx.doi.org/10.1016/0375-9474(68)90893-2.

Bliss, J., Arcones, A., Montes, F., Pereira, J., 2017. Impact of (α,n) reactions on weak r-process in neutrino-driven winds. J. Phys. G: Nucl. Part. Phys. 44, 054003. http://dx.doi.org/10.1088/1361-6471/aa63bd.

Bliss, J., Arcones, A., Montes, F., Pereira, J., 2020. Nuclear physics uncertainties in neutrino-driven, neutron-rich supernova ejecta. Phys. Rev. C 101, 055807. http://dx.doi.org/10.1103/PhysRevC.101.055807.

Bonheure, G., Hult, M., González de Orduña, R., Vermaercke, P., Murari, A., Popovichev, S., Mlynar, J., 2011. Fusion alpha loss diagnostic for ITER using activation technique. Fusion Eng. Des. 86, 1298–1301. http://dx.doi.org/10.1016/j.fusengdes.2011.03.007, Proceedings of the 26th Symposium of Fusion Technology (SOFT-26).

Brandenburg, K., Hamad, G., Meisel, Z., Brune, C.R., Carter, D.E., Derkin, J., Ingram, D.C., Jones-Alberty, Y., Kenady, B., Massey, T.N., Saxena, M., Soltesz, D., Subedi, S.K., Warren, J., 2023. Measurements of the ^{27}Al$(\alpha,n)^{30}$P thick target yield near threshold. Nucl. Sci. Eng. 197, 510–516. http://dx.doi.org/10.1080/00295639.2022.2118483.

Brandenburg, K., et al., 2022. The $^{3}HeBF_{3}$ giant barrel (HeBGB) neutron detector. J. Instrum. 17, P05004. http://dx.doi.org/10.1088/1748-0221/17/05/P05004.

CAEN, S., 2025. DT5533EN 14-bit 500 MS/s 8-Ch digitizer. https://www.caen.it/products/dt5533e/.

Cano-Ott, D., Cebrián, S., Dimitriou, P., Gromov, M., Harańczyk, M., Kish, A., Kluck, H., Kudryavtsev, V.A., Lazanu, I., Lozza, V., Luzón, G., Mendoza, E., Parvu, M., Pesudo, V., Pocar, A., Santorelli, R., Selvi, M., Westerdale, S., Zuzel, G., 2024. White paper on (α, n) neutron yield calculations. http://dx.doi.org/10.48550/ARXIV.2405.07952.

Cerjan, C.J., Bernstein, L., Hopkins, L.B., Bionta, R.M., Bleuel, D.L., Caggiano, J.A., Cassata, W.S., Brune, C.R., Fittinghoff, D., Frenje, J., Gatu-Johnson, M., Gharibyan, N., Grim, G., Hagmann, C., Hamza, A., Hatarik, R., Hartouni, E.P., Henry, E.A., Herrmann, H., Izumi, N., Kalantar, D.H., Khater, H.Y., Kim, Y., Kritcher, A., Litvinov, Y.A., Merrill, F., Moody, K., Neumayer, P., Ratkiewicz, A., Rinderknecht, H.G., Sayre, D., Shaughnessy, D., Spears, B., Stoeffl, W., Tommasini, R., Yeamans, C., Velsko, C., Wiescher, M., Couder, M., Zylstra, A., Schneider, D., 2018. Dynamic high energy density plasma environments at the national ignition facility for nuclear science research. J. Phys. G: Nucl. Part. Phys. 45, http://dx.doi.org/10.1088/1361-6471/aa8693.

Flynn, D.S., Sekharan, K.K., Hiller, B.A., Laumer, H., Weil, J.L., Gabbard, F., 1978. Cross sections and reaction rates for ^{23}Na(p,n), ^{27}Al(p,n), ^{27}Al(α,n), ^{29}Si(α,n), and ^{30}Si(α,n). Phys. Rev. C 18, 1566–1576. http://dx.doi.org/10.1103/PhysRevC.18.1566, URL https://link.aps.org/doi/10.1103/PhysRevC.18.1566.

Fraile, L.M., et al., 2026. Commissioning of the CMAM NUC45 beam line. (in preparation).

Gehrke, R.J., Baker, J.D., Hartwell, J.K., Riddle, C.L., McGrath, C.A., 2003. Measurement of neutron-to-gamma-ray production ratios from (α,n) reactions for their application to assay TRU waste. Nucl. Instrum. Methods Phys. Res. Sect. A 511, 444–456. http://dx.doi.org/10.1016/S0168-9002(03)02011-4.

Heaton, R.K., Lee, H.W., Robertson, B.C., Norman, E.B., Lesko, K.T., Sur, B., 1997. α-Particle induced γ-ray transitions in light elements. Phys. Rev. C 56, 922–937. http://dx.doi.org/10.1103/PhysRevC.56.922.

Heaton, R., Lee, H., Skensved, P., Robertson, R.G.H., 1995. Alpha-particle induced gamma-ray backgrounds in materials commonly used in low-background experiments. Nucl. Instrum. Methods Phys. Res. Sect. A 354, 114–124. http://dx.doi.org/10.1016/0168-9002(95)00220-0.

Herman, M., Capote, R., Carlson, B.V., Obložinský, P., Sin, M., Trkov, A., Wienke, H., Zerkin, V., 2007. EMPIRE: Nuclear reaction model code system for data evaluation. Nucl. Data Sheets 108 (12), 2655–2715. http://dx.doi.org/10.1016/j.nds.2007.11.003.

Holmqvist, B., Ramström, E., 1986. The excitation function of the ^{27}Al(α, n)^{30}p reaction and its astrophysical application. Phys. Scr. 33, 107–109. http://dx.doi.org/10.1088/0031-8949/33/2/003.

Howard, A.J., Jensen, H.B., Rios, M., Fowler, W.A., Zimmerman, B.A., 1974. Measurement and theoretical analysis of some reaction rates of interest in silicon burning. Astrophys. J. 188, 131. http://dx.doi.org/10.1086/152694.

Koning, A.J., Rochman, D., Sublet, J.-C., Dzysiuk, N., Fleming, M., van der Marck, S., 2019. TENDL: Complete nuclear data library for innovative nuclear science and technology. Nucl. Data Sheets 155, 1–55. http://dx.doi.org/10.1016/j.nds.2019.01.002.

Krane, K.S., Steffen, R.M., Wheeler, R.M., 1973. Directional correlations of Gamma radiations emitted from nuclear states oriented by nuclear reactions. 11, (4–5), pp. 351–406. http://dx.doi.org/10.1016/S0092-640X(73)80009-3,

Mei, D.-M., Zhang, C., Hime, A., 2009. Evaluation of (α,n) induced neutrons as a background for dark matter experiments. Nucl. Instrum. Methods Phys. Res. Sect. A: Accel. Spectrometers Detect. Assoc. Equip. 606, 651–660. http://dx.doi.org/10.1016/j.nima.2009.04.032.

Mohr, P., 2015. Cross sections of α-induced reactions for targets with masses A ≈ 20–50 at low energies.. Eur. Phys. J. A 51, 56. http://dx.doi.org/10.1140/epja/i2015-15056-5.

Mont-Geli, N., et al., 2026. Design and commissioning of the miniBELEN neutron counter for the study of (α,n) reactions. accepted.

Mont-Geli, N., Tarifeño-Saldivia, A., Fraile, L., Viñals, S., Perea, A., Pallàs, M., Cortés, G., Garcia, G., Nácher, E., Tain, J., Alcayne, V., Alonso-Sañudo, O., Algora, A., Balibrea-Correa, J., Benito, J., Borge, M., Briz, J., Calviño, F., Cano-Ott, D., De Blas, A., Domingo-Pardo, C., Fernández, B., Garcia, R., Gómez-Camacho, J., González-Romero, E., Guerrero, C., Lerendegui-Marco, J., Llanos, M., Martínez, T., Martínez-Nouvilas, V., Mendoza, E., Murias, J., Orrigo, S., Pérez de Rada, A., Pesudo, V., Plaza, J., Quesada, J., Sánchez, A., Sánchez-Tembleque, V., Santorelli, R., Tengblad, O., Udías, J., Villamarín, D., 2023a. Commissioning of minibelen-10a, a moderated neutron counter with a flat efficiency for thick-target neutron yields measurements. EPJ Web Conf. 290, 01003. http://dx.doi.org/10.1051/epjconf/202329001003.

Mont-Geli, N., Tarifeño-Saldivia, A., Fraile, L., Viñals, S., Perea, A., Pallàs, M., Cortés, G., Nácher, E., Tain, J., Alcayne, V., Algora, A., Balibrea-Correa, J., Benito, J., Borge, M., Briz, J., Calviño, F., Cano-Ott, D., De Blas, A., Domingo-Pardo, C., Fernández, B., Garcia, R., García, G., Gómez-Camacho, J., González-Romero, E., Guerrero, C., Lerendegui-Marco, J., Llanos, M., Martínez, T., Mendoza, E., Murias, J., Orrigo, S., Pérez de Rada, A., Pesudo, V., Plaza, J., Quesada, J., Sánchez, A., Sánchez-Tembleque, V., Santorelli, R., Tengblad, O., Udías, J., Villamarín, D., 2023b. miniBELEN: A modular neutron counter for (reactions. EPJ Web Conf. 284, 06004. http://dx.doi.org/10.1051/epjconf/202328406004.

National Nuclear Data Center, 2025. Evaluated Nuclear Structure Data File (ENSDF). Retrieved from https://www.nndc.bnl.gov/ensdf.

Redondo-Cubero, A., Borge, M.J.G., Gordillo, N., Gutiérrez, P.C., Olivares, J., Pérez Casero, R., Ynsa, M.D., 2021. Current status and future developments of the ion beam facility at the centre of micro-analysis of materials in Madrid. Eur. Phys. J. Plus 136, 175. http://dx.doi.org/10.1140/epjp/s13360-021-01085-9.

Roughton, N., Intrator, T., Peterson, R., Zaidins, C., Hansen, C.J., 1983. Thick-target measurements and astrophysical thermonuclear reaction rates: Alpha-induced reactions. At. Data Nucl. Data Tables 28 (2), 341–353. http://dx.doi.org/10.1016/0092-640X(83)90021-9.

Roy, R., Testov, D.A., Balabanski, D.L., Kaur, M., Kuşğlu, A., Lorusso, G., Singh, S., Söderström, P.-A., Xu, Y., Aogaki, S., Ban, S.-R., Brezeanu, M., Burducea, I., Corbu, R., Cuciuc, M., Dhal, A., Djourelov, N., Florea, N., Gavrilescu, A., Gheorghiu, C., Guardo, G.L., Iancu, D., Lelasseux, V., Nedelcu, C.V., Pai, H., Parlea, P., Petruse, T., Rotaru, A., State, A.N., Straticiuc, M., Toma, V., Tozar, T., Choudhury, D., 2025. α-Induced neutron emission from ^{27}Al: A cross-section study. Phys. Rev. C 112, 044613. http://dx.doi.org/10.1103/6r82-456g.

Sahakundu, S., Qaim, S., Stöcklin, G., 1979. Cyclotron production of short-lived ^{30}P. Int. J. Appl. Radiat. Isot. 30, 3–5. http://dx.doi.org/10.1016/0020-708X(79)90088-7.

Seyler, R.G., Weller, H.R., 1979. Angular distribution theory for particle-capture γ reactions. Phys. Rev. C 20, 453–460. http://dx.doi.org/10.1103/PhysRevC.20.453.

Stelson, P.H., McGowan, F.K., 1964. Cross sections for (α,n) reactions for medium-weight nuclei. Phys. Rev. J. 133, B911–B919. http://dx.doi.org/10.1103/PhysRev.133.B911.

Struck Innovative Systeme, 2012. SIS3316 16 channel VME digitizer family. https://www.struck.de/sis3316.html.

Subedi, S.K., Meisel, Z., Merz, G., 2020. Sensitivity of ^{44}Ti and ^{56}Ni production in core-collapse supernova shock-driven nucleosynthesis to nuclear reaction rate variations. Astrophys. J. 898, 5. http://dx.doi.org/10.3847/1538-4357/ab9745.

Tain, J.L., Jordán, D., Agramunt, J., Algora, A., Bandac, I., Bettini, A., Caballero-Folch, R., Calviño, F., Cano-Ott, D., Cortés, G., Domingo-Pardo, C., Fraile, L.M., García, A.R., Gomez-Cadenas, J.J., José, J., Longland, R., Mendoza, E., Parikh, A., 2016. Measurement of very low (α,n) cross sections of astrophysical interest. J. Phys.: Conf. Ser. 665, 012031. http://dx.doi.org/10.1088/1742-6596/665/1/012031.

Thermo Fisher Scientific, 0000. URL https://www.thermofisher.com/es/es/home.html.

Vedia, V., Carmona-Gallardo, M., Fraile, L.M., Mach, H., 2017. Performance evaluation of novel $LaBr_3$(Ce) scintillator geometries for fast-timing applications. Nucl. Instrum. Methods Phys. Res. Sect. A: Accel. Spectrometers Detect. Assoc. Equip. 857, http://dx.doi.org/10.1016/j.nima.2017.03.030.

Vlaskin, G.N., Khomyakov, Y.S., Bulanenko, V.I., 2015. Neutron yield of the reaction (α,n) on thick targets comprised of light elements. At. Energy 117, 357–365. http://dx.doi.org/10.1007/s10512-015-9933-5.

Wang, M., Huang, W.J., Kondev, F.G., Audi, G., Naimi, S., 2021. The AME 2020 atomic mass evaluation (II). Tables, graphs and references. Chinese Phys. C 45, 030003. http://dx.doi.org/10.1088/1674-1137/abddaf.

West, D., Sherwood, A., 1982. Measurements of thick-target (α,n) yields from light elements. Ann. Nucl. Energy 9, 551. http://dx.doi.org/10.1016/0306-4549(82)90001-9.

Westerdale, S., Junghans, A., deBoer, R.J., Pigni, M., Dimitriou, P., 2022. (α,n) Nuclear Data Evaluations and Data Needs: Summary Report of the Technical Meeting. Tech. rep., International Atomic Energy Agency (IAEA), Available from the IAEA Nuclear Data Section.

Williamson, R.M., Katman, T., Burton, B.S., 1960. ^{19}F, ^{23}Na, and ^{27}Al (α,n) reactions. Phys. Rev. J. 117, 1325–1329. http://dx.doi.org/10.1103/PhysRev.117.1325.

Wilson, W., Perry, R., Charlton, W., Parish, T., 2009. Sources: A code for calculating (α, n), spontaneous fission, and delayed neutron sources and spectra. Prog. Nucl. Energy 51, 608–613. http://dx.doi.org/10.1016/j.pnucene.2008.11.007.

Ziegler, J.F., Ziegler, M., Biersack, J., 2010. SRIM – the stopping and range of ions in matter. Nucl. Instruments Methods Phys. Res. Sect. B: Beam Interactions Mater. Atoms 268 (11), 1818–1823. http://dx.doi.org/10.1016/j.nimb.2010.02.091, 19th International Conference on Ion Beam Analysis.